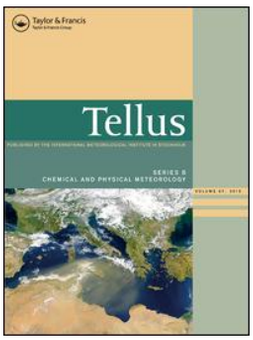

Tellus B: Chemical and Physical Meteorology

ISSN: (Print) 1600-0889 (Online) Journal homepage: http://www.tandfonline.com/loi/zelb20

Very low ozone episodes due to polar vortex displacement

P. M. James, D. Peters & D. W. Waugh

To cite this article: P. M. James, D. Peters & D. W. Waugh (2000) Very low ozone episodes due to polar vortex displacement, Tellus B: Chemical and Physical Meteorology, 52:4, 1123-1137, DOI: 10.3402/tellusb.v52i4.17089

To link to this article: https://doi.org/10.3402/tellusb.v52i4.17089

Published online: 15 Dec 2016.

Tellus (2000), 52B, 1123–1137
Printed in UK. All rights reserved

TELLUS
ISSN 0280–6509

Very low ozone episodes due to polar vortex displacement

By P. M. JAMES[1], D. PETERS[1]* and D. W. WAUGH[2], [1]*Leibniz-Institut für Atmosphärenphysik, Kühlungsborn, Germany;* [2]*Department of Earth and Planetary Sciences, Johns Hopkins University, Baltimore, USA*

(Manuscript received 23 August 1999; in final form 13 December 1999)

ABSTRACT

The large-scale ozone distribution over the northern hemisphere undergoes strong fluctuations each winter on timescales of up to a few weeks. This is closely linked to changes in the stratospheric polar vortex, whose shape, intensity and location vary with time. Elliptical diagnostic parameters provide an empirical description of the daily character of the polar vortex. These parameters are used as an objective measure to define two characteristic wintertime vortex displacements, towards northern Europe and Canada, respectively. The large-scale structures in both the stratosphere and troposphere and the 3D ozone structures are determined for both vortex displacement scenarios. A linear ozone transport model shows that the contribution of horizontal ozone advection dominates locally in the middle stratosphere. Nevertheless, the largest contribution is due to vertical advection around the ozone layer maximum. The findings are in agreement with an EOF analysis which reveals significant general modes of ozone variability linked to polar vortex displacement and to phase-shifted large-scale tropospheric waves. When baroclinic waves travel through the regions of vortex-related ozone reduction, the combined effect is to produce transient synoptic-scale areas of exceptionally low ozone; namely dynamically induced strong ozone mini-holes.

1. Introduction

The distribution of ozone over the northern hemisphere exhibits considerable variability on a wide range of temporal and spatial scales. Short-term, synoptic ozone variations are primarily associated with the passage of tropospheric weather systems (Dobson et al., 1929; Reed, 1950), chiefly in mid-latitudes. In particular, transient regions of strongly depleted ozone can occur, referred to as ozone mini-holes (Newman et al., 1988; McKenna et al., 1989; Peters et al., 1995), formed primarily by local airmass ascent across the tropopause region resulting in divergence of ozone rich stratospheric air out of the column (Rood et al., 1992; James et al., 1997). Meanwhile on the large scale, the hemispheric distribution of ozone is strongly influenced by transports involving ultra-long waves (Kurzeja, 1984). Hence, even without the additional role of long-term zonally asymmetric trends (Peters and Entzian, 1999) and the interannual and intraseasonal variability (Greisiger et al., 1998), the day-to-day total ozone variability is derived from a superposition of effects. Similarly, while mini-holes of moderate strength occur throughout the storm-track regions of the hemisphere (James, 1998), very intense mini-holes are typically observed in combination with some strongly disturbed circulation pattern in the stratosphere. For example, Petzoldt et al. (1994), Petzoldt (1999) have shown case-studies in which exceptionally deep mini-holes occurred over northern Europe during stratospheric warming

* Corresponding author. Address: Leibniz-Institut für Atmosphärenphysik, Schloßstraße 6, D-18225 Ostseebad Kühlungsborn, Germany.
e-mail: peters@iap-kborn.de

episodes. The primary characteristic of such stratospheric warmings is a strong displacement of the polar vortex cold pool away from pole, usually towards north-east Europe and Siberia, allowing a strong warm anomaly to form over the pole and arctic Canada in particular.

Displacement and deformation of the polar vortex, an expression of its considerable variability, is indeed frequent, contrasting strongly with the relatively stable vortex over the Antarctic. The "Berliner Phänomen" (Scherhag, 1952), a strong local warming in the stratosphere, is one example of this variability. Erosion of the polar vortex through breaking Rossby-waves (McIntyre and Palmer, 1983) has also been observed, as have strong intrusions in connection with processes leading to polar vortex breakdown (Plumb et al., 1994). In all such cases, wide-reaching disturbances of the stratospheric circulation are seen, resulting in large changes in ozone transport fluxes. Hence, it is clear that displacements of the polar vortex are likely to have a significant effect on hemispheric ozone distributions, not only in special cases such as stratospheric warmings, but also in general.

A new and effective method of describing the character of the polar vortex are the Elliptical Diagnostics (EDs) of Waugh (1997). The EDs can be used to quantify the size, shape and locations of the polar vortices. Using these diagnostics Waugh and Randel (1999) formed a climatology of the structure of the Arctic and Antarctic vortices, and examined the climatological mean structure as well as the interannual variability.

The goal of this paper is to use the ED-approach to characterize the dynamically induced 3D ozone structures during observed polar vortex displacements and to determine the associated configurations of the large-scale stratospheric- and, in turn, tropospheric circulations. The relative contributions of horizontal and vertical advection to the total ozone changes at various altitudes during vortex displacements will be determined through the use of a simple linear transport model for ultra-long waves. A general basis for understanding how the additional passage of a baroclinic system through a vortex-induced low ozone region can produce transient extremely low ozone levels, as in the Petzoldt case studies, can then be formed.

The data used are described in Section 2. The ED methodology is introduced in Section 3 and composite fields are shown for various generalised types of vortex displacements. Transport model calculations, based on these vortex displacement scenarios, are shown in Section 4. An ozone-weighted EOF analysis of the stratospheric and tropospheric circulations is presented in Section 5, while discussions and conclusions are drawn in Section 6.

2. Data

ECMWF-Reanalysis data for ten winters (DJF), covering the period December 1982 to February 1992 inclusive, are employed to provide the daily meteorological fields for this study. The quantities used are geopotential, temperature and zonal wind, stored at a reduced resolution of 6° latitude $\times$ 5° longitude, adequate for the study of large-scale atmospheric structures. In the vertical, the data are available on 17 pressure levels: 11 in the troposphere and 6 in the stratosphere, the highest being at 10 hPa. Daily ozone data is provided by total column ozone observations from the Nimbus-7 TOMS instrument, version 7, interpolated onto the same grid as above and covering the same ten year period. The elliptical diagnostics of the stratospheric circulation are derived from daily NCEP stratospheric analyses (Randel, 1992).

3. Composites based on elliptical diagnostics of the polar vortex

A new and efficient method of describing the behaviour of the stratospheric polar vortex, using a set of basic parameters known as Elliptical Diagnostics, has been constructed by Waugh (1997). Daily Ertel's Potential Vorticity (PV) (Ertel, 1942) fields on a set of reference isentropes in the middle to upper stratosphere were examined. At any of these levels, the polar vortex is characterised as a large area of relatively high PV in polar regions, typically with sharp PV gradients at its boundaries, with significantly lower PV surrounding it in middle latitudes. On each isentrope, an optimal PV value may be chosen as being typically representative of the vortex edge. The contour of this PV value is traced for each day, forming a meandering, wavy circuit, centred somewhere in the polar regions, having broadly

Table 1

Scenario	Equiv. area*	Centre (lat, long)	Aspect ratio	No. indep. events (days)
EVS	$>15.0^\circ$	$<75^\circ$, 15°E–60°E	<1.50	10 (19)
CVS	$>12.5^\circ$	$<80^\circ$, 120°W–45°W	<1.50	10 (23)

* Equivalent area is the surface area of the vortex, expressed as an inverse latitude, this being the number of degrees latitude from the pole that the edge of the vortex would reach if it were made circular and centred exactly over the pole. Hence, a 15° equivalent area vortex would reach to 75°N if it were thus relocated and reshaped.

an elliptical form. To simplify matters and produce a useable dataset, Waugh (1997) superimposed a basic ellipse over the actual vortex edge, estimating this using an objective best-fit method. The character of the ellipse is represented by a set of parameters (the so-called EDs) defining its surface area, the position of its centre, its aspect ratio and the orientation of its major axis relative to the Greenwich meridian. The EDs can then be used to quantify the vortex structure. Note that one limitation of the EDs is that a single ellipse is used to characterise the vortex and so they cannot adequately represent situations when the vortex splits into two fragments, such as during stratospheric warmings; although it would be possible in principle to calculate EDs for both fragments in such a case.

For this study, we use the 500 K EDs from Waugh and Randel (1999) to estimate the structure and behaviour of the Arctic polar vortex. The 500 K isentrope is used as there is a strong vortex at this level throughout the Dec.–Feb. period. To show structures associated with a polar vortex displacement, we have constructed mean composite fields based on various specified vortex scenarios. Several scenarios have been tested, each based on quite different configurations of the ED parameters, yielding a range of broadly consistent results. Of these, we present two scenarios of particular interest: cases in which the vortex shifts off the pole while remaining strongly intact.

In the first scenario, the polar vortex is displaced towards north-east Europe and north-west Russia, while remaining intense and broadly circular, referred to as the "European Vortex Shift" scenario (EVS for short). This is of particular interest, since this type of vortex displacement has been connected to cases of strong ozone mini-hole events over northern Europe (Petzoldt et al., 1994). In a second, comparative scenario, the "Canadian Vortex Shift" (CVS for short), the vortex is displaced towards arctic Canada. The precise definition of these cases is given in Table 1, above. All 900 days in the available dataset are examined, and those on which the vortex passes all of the respective parameter tests are used in constructing the relevant composites. The total number of days on which each scenario occurred is indicated in the table. Since the vortex may remain stable within a scenario definition for a few days at a time, the number of independent events counting towards each scenario composite is also shown. The sensitivity of the results to small variations in the parameter tests given in table has also been tested. While a certain level of arbitrariness in setting the parameter thresholds is hard to avoid, the results appear to be qualitatively robust.

Composite fields of geopotential at 30 hPa and 300 hPa, expressed in absolute form and as anomalies from respective monthly climatological normals, and of column total ozone are shown for scenario EVS in Fig. 1. At 30 hPa, the geopotential field shows up the displacement of the polar vortex explicitly. A strong negative geopotential anomaly lies near 30°E, 60°N, while an equally strong positive anomaly is seen over arctic Canada. In the upper troposphere, however, a significant anticyclonic ridging is in evidence, with anomaly values approaching 30 dam north-west of Europe near 15°W, on the western flank of the stratospheric polar vortex. Almost exactly mid-way between the upper and lower geopotential anomaly centres is a very strong negative ozone anomaly, centred squarely over north-west Europe near 5°E, exceeding -60 DU. This signal is highly statistically significant, exceeding even the 99% confidence level near its centre and is strong enough to leave the total field with a mean closed area of low ozone over northern Europe. In the

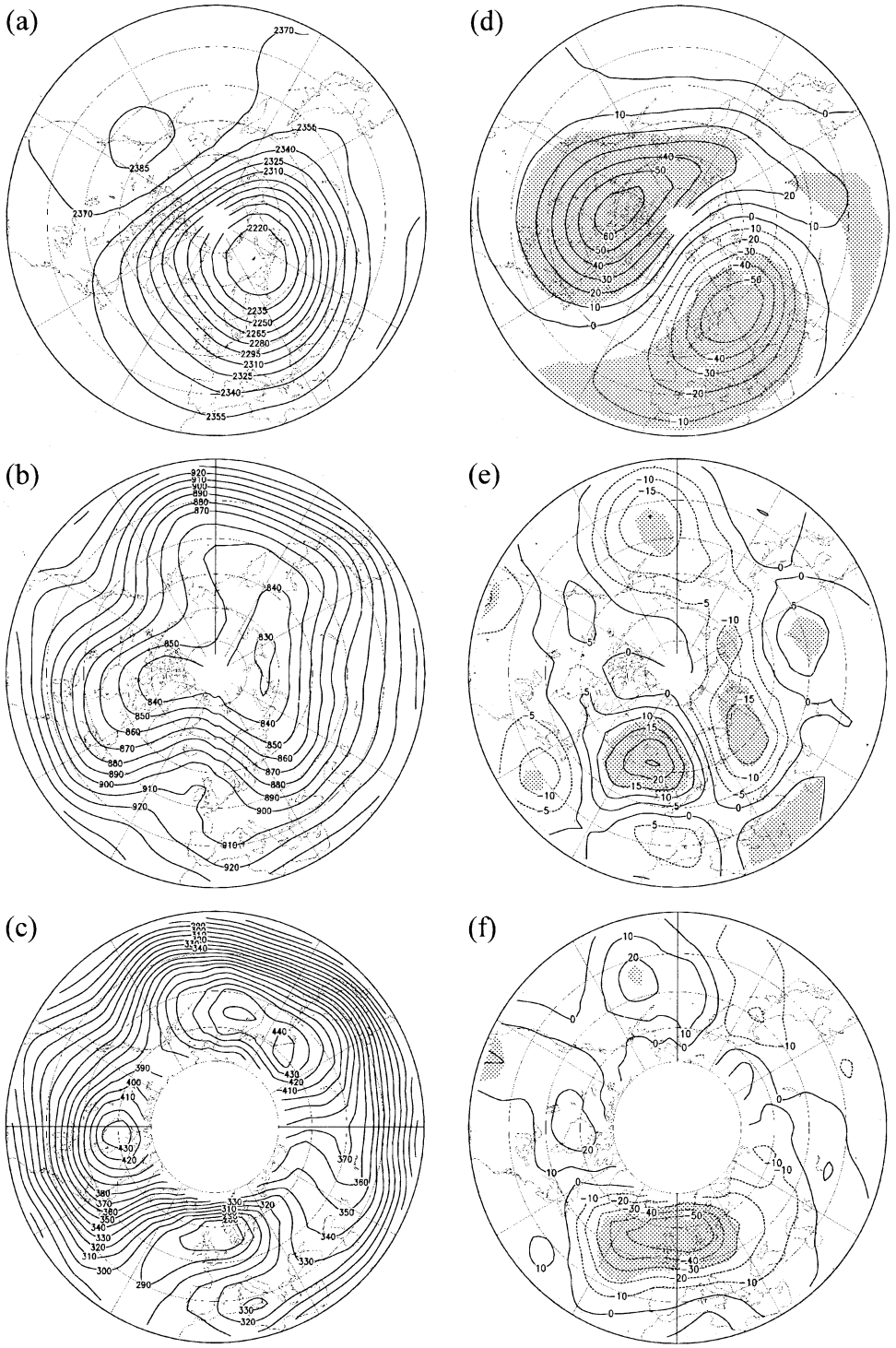
(a)
(d)
(b)
(e)
(c)
(f)

other regions of the hemisphere, weak positive ozone anomalies are seen.

The equivalent pictures for scenario CVS are shown in Fig. 2. At 30 hPa, a strong dipolar geopotential anomaly pair is associated with the shift of the polar vortex into arctic Canada. Indeed the positive part of the anomaly pattern is especially large, so that only a remnant of the climatological vortex is left over arctic Siberia in the total field. Unlike the EVS above, significant CVS anomalies at the 300 hPa level are only seen along the vortex displacement axis itself, although the anomalies show the same geographical relationship, relative to the vortex, as above: cyclonic under and to the east of the vortex, enhanced westerly flow south-east of the vortex, anticyclonic on the western flank of the vortex. The climatological ridging along the north Pacific coastline is enhanced slightly in the CVS scenario, but the signal is not significant. However, the CVS dipolar ozone anomaly signal is again highly significant. A strong negative anomaly, approaching -70 DU in its centre, dominates the North American continent. Just as in the EVS case, this ozone anomaly is found mid-way between the local geopotential anomalies at the two respective pressure levels. Meanwhile the European–Siberian landmasses see a positive anomaly exceeding $+40$ DU in places. The CVS ozone anomalies are generally more zonally extensive than the more compact EVS equivalents.

The robustness of the respective composite ozone patterns have been tested against possible systematic errors due to the long-term ozone trends as well as the seasonal cycle of mean ozone which is in a phase of rapid increase between December and February. The composites have been reproduced using de-trended ozone data and with a sinusoidally modelled mean seasonal ozone cycle; the latter producing a slightly more accurate climate background state than when using monthly mean climate fields. However, neither of these adjustments has any significant effect on the character of the composites. We note that the zonal means of the composited ozone anomalies are generally small, not exceeding ± 10 DU on any latitude band and with hemispheric means of less than ± 2 DU.

The results confirm that polar vortex displacements and their associated dynamical structures correlate with significant anomaly patterns of the hemispheric ozone distribution. It can be supposed that changes in both the polar vortex and in upper tropospheric waves play a role in the ozone changes. However, it is not yet clear what relative importance these two factors play, or what proportion of the ozone anomalies are due to vertical advection in comparison with horizontal advection.

4. Transport model calculations

To tackle the question above, we now investigate the advection contributions of the large-scale wave structure to the ozone distribution, concentrating on the polar vortex displacement scenarios EVS and CVS discussed earlier.

Composite fields of the respective large-scale structure of the long waves associated with each scenario are derived. Then, on the basis of a linear transport model (1), the zonally asymmetric ozone distribution, η^* is computed. This model is described in detail in, e.g., Peters et al. (1996) and is only briefly reintroduced here.

$$\frac{[U]\eta^*_\lambda}{a\cos\varphi} = -\frac{v^*}{a}[\eta]_\varphi - w^*[\eta]_z, \qquad (1)$$

where z is the vertical coordinate, λ the longitude, φ the latitude and a the radius of the earth.

The meridional and vertical velocity fields, v^* and w^* are calculated from the geopotential composites, via the geostrophic balance relation and the energy equation with no heat source. The zonally averaged quantities, static stability and zonal wind $[U]$, are based on climatological averages from the ECMWF-reanalyses. $[\eta]$ was chosen as the mean ozone distribution for the winter 1978/79 (McPeters et al., 1984). This was derived by averaging the three monthly-mean fields for

Fig. 1. Polar stereographic plots over the northern hemisphere down to 30°N during EVS events in winter (DJF). Geopotential composites on (a) the 30 hPa pressure level, contour interval 15 dam, (b) the 300 hPa pressure level, contour interval 10 dam; with (c) total column ozone, contour interval 10 DU. (d–f) show the anomalies from winter climate normals of the respective (a–c) fields, contour intervals 10 dam, 5 dam and 10 DU, respectively. Negative contours dashed, shaded areas represent regions where the anomalies exceed the 95% confidence level.

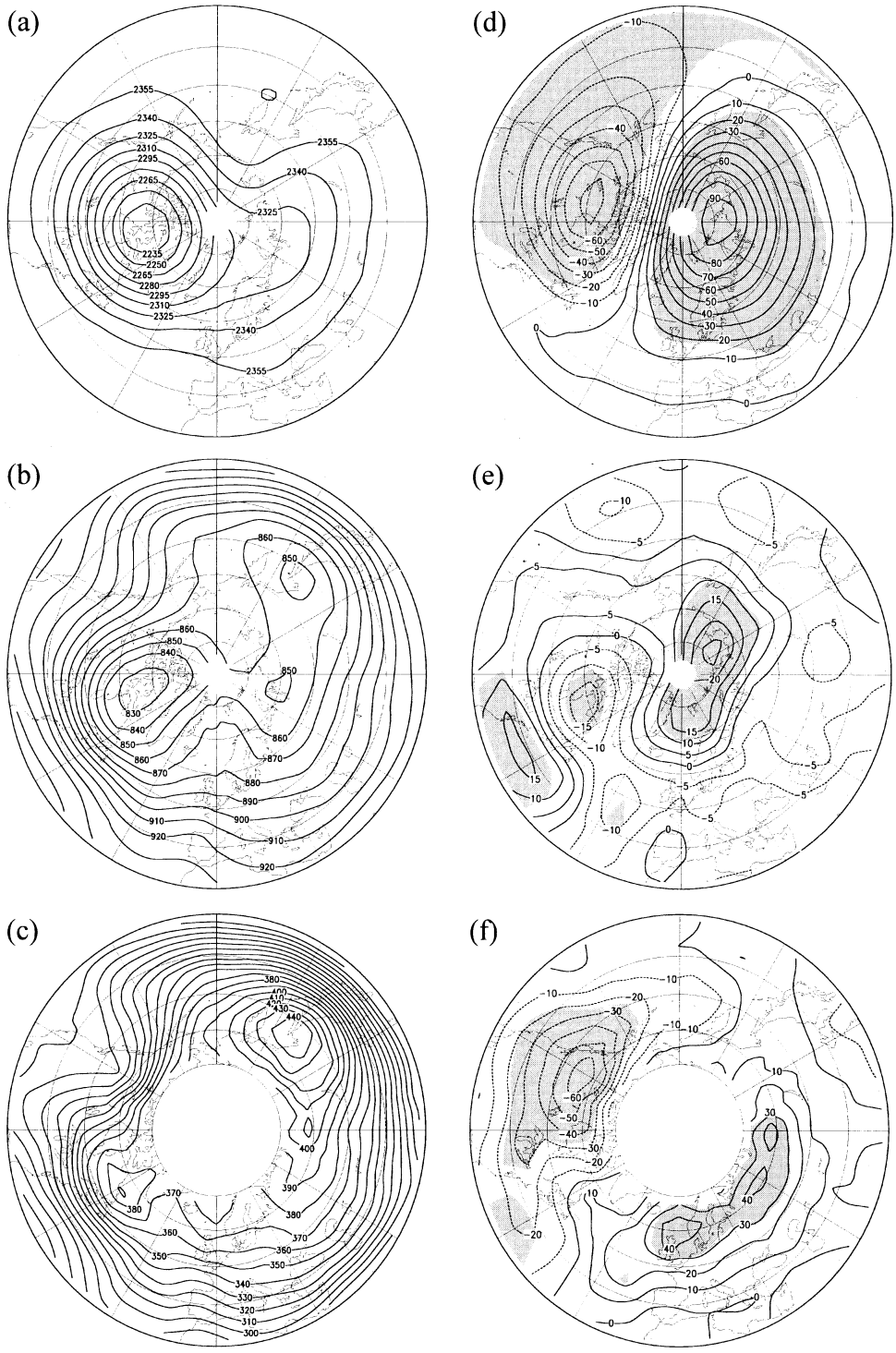

Fig. 2. As Fig. 1 but for the CVS scenario.

December, January and February together, extrapolating up to 90°N to fill the data gaps due to the polar night in mid-winter, and is shown in Fig. 3. Strong horizontal as well as vertical ozone gradients exist in the mid-latitudes of both hemispheres. The signs of these gradients all reverse on crossing the axis of maximum ozone. The McPeters dataset was chosen in preference to other climatological ozone measurements, such as from SAGE or UARS satellites, since it is one of the highest quality and most spatially extensive available below the ozone layer maximum. Only climatological ozone gradients, not absolute ozone levels, play a role for the transport model results. The potential influence of the zonal mean trend has been tested (Peters et al., 1996) and shown to induce uncertainties of no more than 10%, which is in any case less than the fundamental accuracy of the transport model itself.

The computed total ozone distribution, along with its separated horizontal and vertical advection contributions, are shown in Fig. 4 for the EVS and CVS composites. In both cases, the results are presented as anomalies from a control run of the model based on climatological geopotential fields. In this way the transport model ozone anomalies can be directly compared with the observed ozone composites for the EVS and CVS scenarios, shown in Figs. 1, 2 respectively.

In the case of EVS, an area of strong ozone reduction occurs over the North Atlantic–European region (max. anomalies ~ -40 DU). This is largely dominated by the contribution from vertical advection, whereas horizontal advection contributes to the ozone reduction only over the Atlantic but increases ozone over the much of the near-continent. Meanwhile total ozone increases are seen in the Pacific/North American region. Maximum ozone anomalies are about $+20$ DU south of the Aleutians where the horizontal advection contribution has the same sign as that from vertical advection. Over North America horizontal advection contribution works against vertical advection contribution leaving only weak total anomalies.

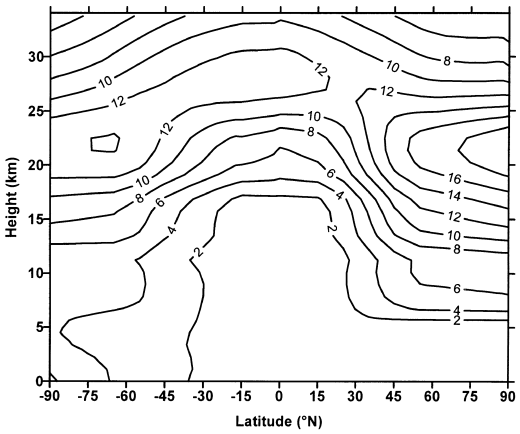

Fig. 3. Mean zonal–mean ozone, recalculated in DU/km for winter 1978/79, contour interval 2 DU/km, based on ozone mixing ratio for each winter month after McPeters et al. (1984) and extrapolated to the poles.

In contrast, the CVS case shows a region of maximum total ozone reduction over western North America (max. ~ -35 DU). This has a similar amplitude to the European anomaly of the EVS case but lies some 10° further south. A zonally extensive area of ozone increase is seen stretching across Europe. Again, the vertical advection contribution dominates the total anomaly field. Similarly to the EVS case, the centres of the weaker horizontal advection contributions are generally phase-shifted in mid-latitudes almost 90° westwards of the respective vertical advection contribution anomalies.

If we compare the modelled total ozone fields for EVS (Fig. 4a) and CVS (Fig. 4d) with the respective composite ozone anomalies shown in Figs. 1f and 2f, we see that in both cases the model describes the anomaly structures quite well. There is a surprisingly good phase relation between composite anomalies and model results. On the other hand, model amplitudes are underestimated by up to 50%. However, we note that the linear model used climate averages of zonal mean zonal wind and temperature as well as mean winter 1978/79 zonal mean ozone field, which could account for the underestimation of the ozone anomaly amplitudes.

In Fig. 5, height–longitude cross-sections through the centres of greatest ozone reduction, as revealed in Fig. 4, are shown at 60°N (EVS) and 50°N (CVS) respectively. These demonstrate the height dependencies of the horizontal and vertical advection contributions at these latitudes to the total contribution. Thus it is possible to estimate the relative importance of the partial advective contributions of the waves at each level during displacements of the polar vortex.

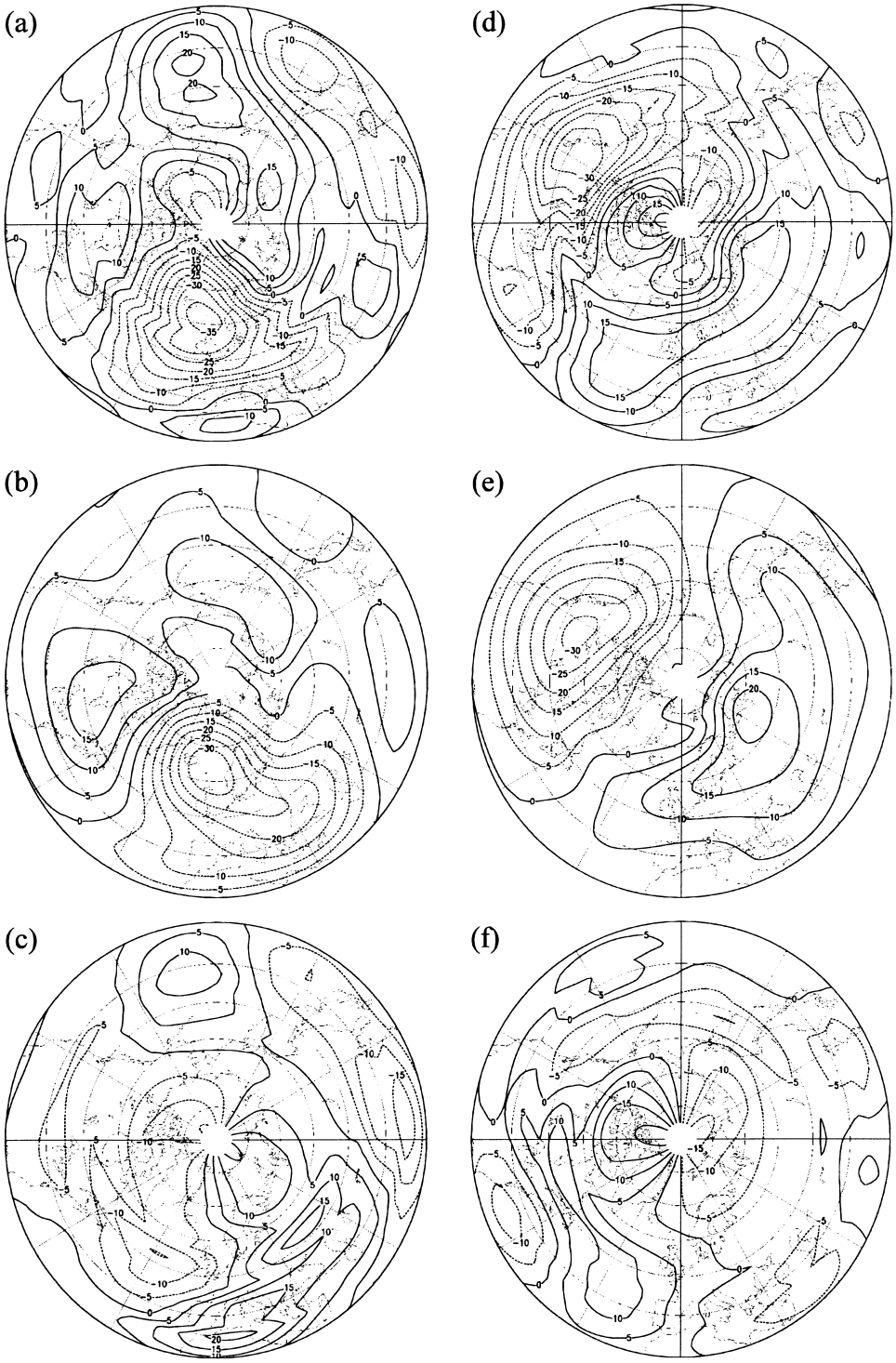
(a)
(d)
(b)
(e)
(c)
(f)

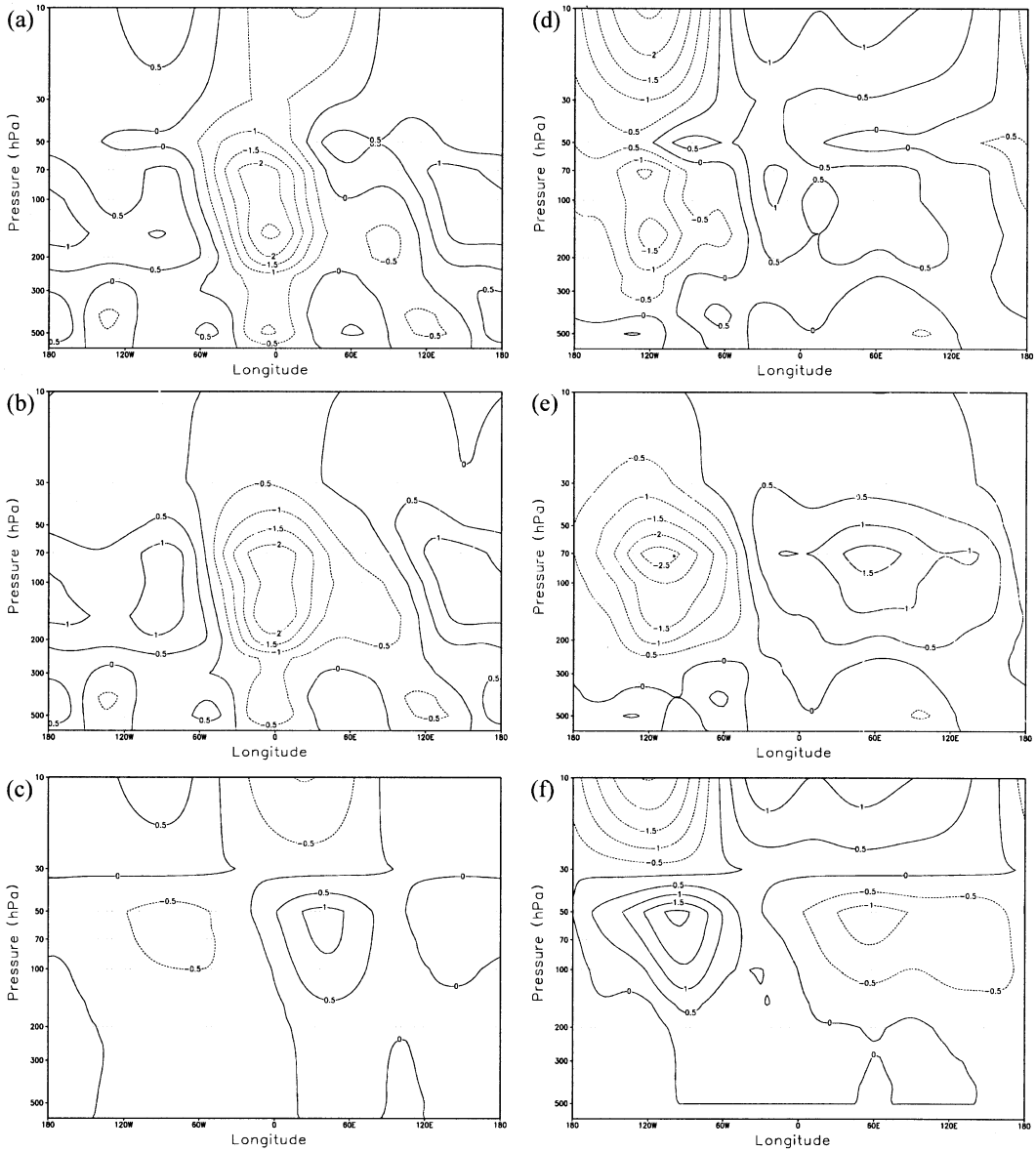

Fig. 5. Height–longitude cross-sections for (a–c) the EVS scenario at 60°N and (d–f) the CVS scenario at 50°N, respectively, of (a,d) total ozone changes in the linear transport model, composed of contributions from (b,e) vertical advection and (c,f) horizontal advection. Contour interval 0.5 DU/km.

Fig. 4. Ozone changes over the northern hemisphere in the linear transport model for (a–c) the EVS scenario and (d–f) the CVS scenario. Shown are (a,d) the total ozone changes, composed of contributions from (b,e) vertical advection and (c,f) horizontal advection. Contour interval 5 DU.

For the EVS case at 60°N, the dominant contribution to the total ozone reduction (Fig. 5a) is found between 250 hPa and 50 hPa in the sector 30°W to 30°E, with a slight westward phase-shift, while a second relative maximum is found between 30 hPa and 10 hPa in the sector 30°W to 60°E. Whereas the vertical advection contribution determines the structure below 250 hPa (Fig. 5c), the horizontal advection term plays an increasingly important role at the higher levels (Fig. 5b). Above 30 hPa, the vertical and horizontal transport contributions are very nearly in phase, but the horizontal part dominates at this latitude. This confirms the importance of horizontal advection contributions above the maximum ozone layer due to the polar vortex, leading to a strong ozone reduction. Underneath this layer, the vertical advection contribution dominates. A cross-section at lower latitudes (not shown), however, reveals that the horizontal transport contribution also plays a significant role in levels between 200 hPa and 30 hPa in midlatitudes.

For the CVS case at 50°N, the total advective ozone change is composed of a contribution of the horizontal advection above 30 hPa near 120°W (Fig. 5e), together with a contribution of the vertical advection concentrated around and below the ozone layer maximum in the sector 150°W to 60°W (Fig. 5f). Below about 30 hPa, the vertical and horizontal advection contributions are almost completely opposite in phase, leaving only weak total ozone anomalies (Fig. 5d), whereas in the middle stratosphere, the two components work together in phase, demonstrating the importance of horizontal ozone advections above the ozone maximum layer by the polar vortex.

5. Field-triplet EOF analysis

The findings above reveal significant ozone structure changes associated with certain predetermined polar vortex displacements. To investigate the general dynamical connection between ozone and the polar vortex, we use a modifed form of EOF analysis to reveal the most significant modes of dynamical variability which couple the middle stratosphere to the upper troposphere while taking ozone further into account. This is hence a generalisation of the scenario-setting approach above; one which counts for any type of polar vortex displacement in any direction.

The EOF analysis is applied to a set of 3 daily fields, placed side-by-side, forming a field-triplet. These are the geopotential at 30 hPa and at 300 hPa, and the column total TOMS ozone. They are input as anomaly fields from climate normal and are each normalised by their mean standard deviations, respectively. The latter ensures that each field contributes the same mean level of variance to the resulting EOFs. The anomaly fields are also weighted by the cosine of latitude, ensuring that each grid-point value contributes to the total relative to its respective surface area. The most important coupled modes between the three fields are thus revealed. In one sense, ozone can be viewed as a weighting factor: the modes revealed which show dynamical coupling between the 30 hPa and 300 hPa levels are weighted to bring out those particular modes which have the most significant effect on the ozone field.

The resulting EOFs are three-component patterns which show how the various fields couple to each other in each case. EOF 1, accounting for 15% of the total variance of the coupled fields and shown in Figs. 6a–c, represents a polar vortex displacement, either towards northern Canada (positive phase) or towards north-east Europe (negative phase). Hence, EOF 1+ resembles the scenario CVS, while EOF 1− resembles the scenario EVS. Concentrating on EOF 1−, in the 300 hPa level, a positive, anticyclonic geopotential anomaly lies to the west of Europe, west of the displaced polar vortex. This is in good agreement with the composite fields derived for scenario EVS. Precisely half-way between the geopotential anomaly centres at the two heights is a negative ozone anomaly, covering much of Europe. Similarly, in the positive phase of EOF 1, reduced ozone over

Fig. 6. Field-triplet EOF patterns over the northern hemisphere, showing (a–c) EOF 1 and (d–f) EOF 2. Shown are the three normalised components of each EOF respectively: (a,d) geopotential at 30 hPa, (b,e) geopotential at 300 hPa and (c,f) column total ozone. Contour interval 0.02, negative contours dashed. The pattern is normalised so that the squares of all grid-point values of all three fields add up to unity.

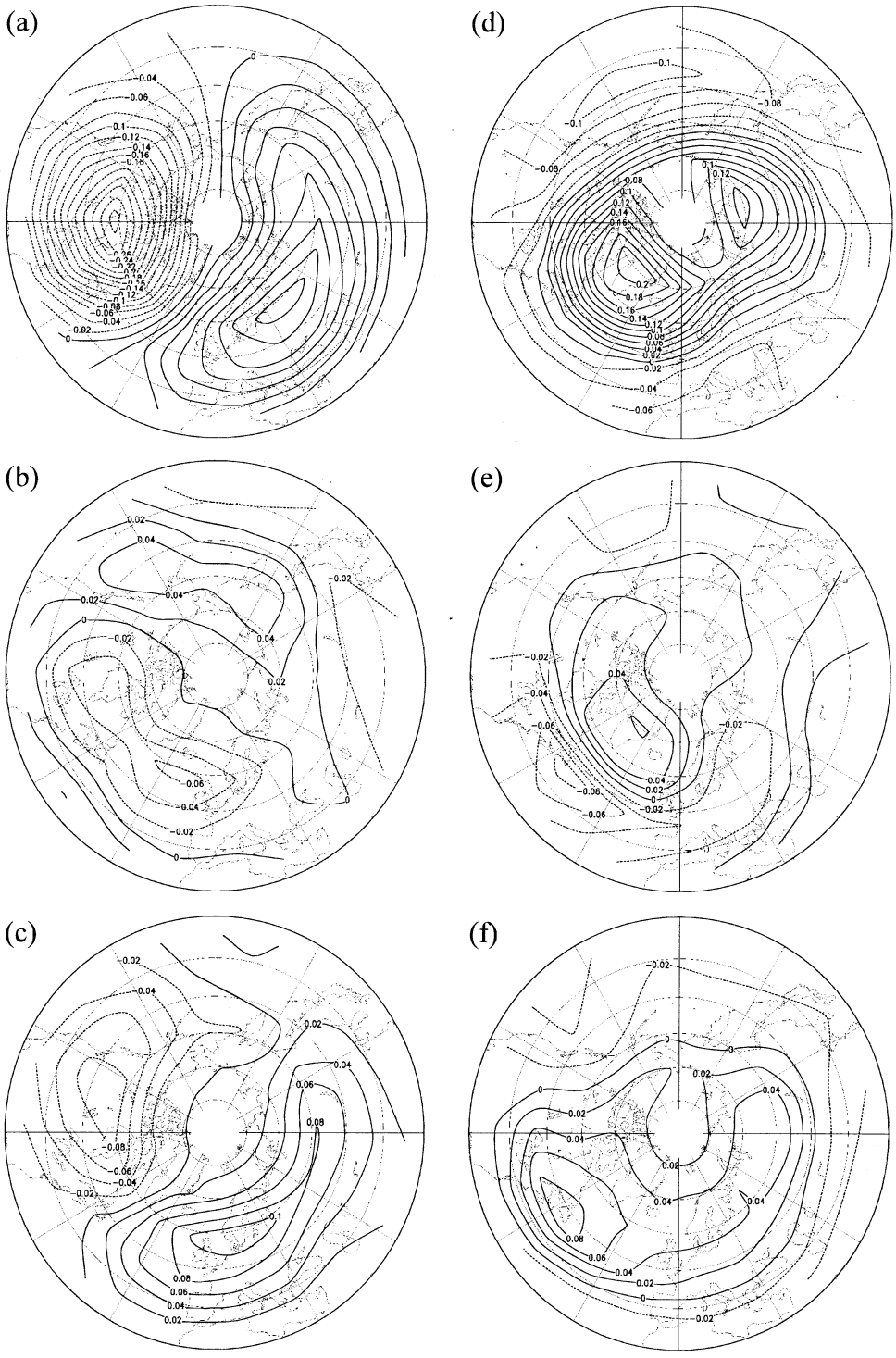
(a)
(d)
(b)
(e)
(c)
(f)

western Canada is seen between anticyclonic tropospheric anomalies in the north-east Pacific and the displaced polar vortex over central Arctic Canada.

EOF 2, shown in Fig. 6d–f, explaining 12% of the total variance, is dominated by the 30 hPa geopotential, such that the polar vortex exhibits an in-situ weakening (strengthening) without displacement. A North-Atlantic Oscillation (NAO) signal is evidenced at the 300 hPa level, for example with enhanced westerly flow under the edge of a strong Arctic polar vortex, while the ozone pattern is weakly positively correlated to the 30 hPa polar vortex signal and further somewhat enhanced in the region of anomalous zonal flow associated with the NAO signal. The EOF 2 pattern in fact closely resembles the so-called Arctic Oscillation pattern recently discussed by Thompson and Wallace (1998) for example. The further EOFs represent vortex displacements in different directions, vortex splitting, and so on. These will not be discussed further here, however.

The EOF 1 pattern confirms that the displacement of the polar vortex along the axis Europe–Canada, coupled with anticyclonic anomalies in the upper troposphere on the western flanks of the shifted vortex, is a major mode of atmospheric variability, having an important effect on ozone levels over Europe, as well as North America.

6. Discussion and summary

Our findings confirm that the displacement of the polar vortex in the wintertime northern hemisphere is a central dynamical factor in determining the structure of the large-scale stratospheric circulation and is strongly coupled to tropospheric circulation changes, which in turn leads to significant and consistent changes in the hemispheric ozone distribution. While the variability of the polar vortex may be influenced by various internal radiative processes, caused by factors such as tropospheric CO_2 increase (Shindell et al., 1999), ozone depletion, or the increase of aerosol contamination (Graf et al., 1998), the primary cause, especially on day-to-day timescales, is undoubtedly dynamical in origin, caused for instance by interactions between planetary waves and the basic flow, as well as through wave–wave interactions.

Our motivation for choosing the particular vortex shift scenarios, EVS and CVS, which could otherwise be seen as somewhat arbitrary, has been given weight by the field-triplet EOF analysis, which has shown that vortex displacement along the Canadian–North-East-European axis is the most common and important displacement mode, with the noted coupling to the tropospheric circulation adding further significance to the findings. Our requirement of nearly circular vortices for the EVS and CVS cases is also supported by the EOF results, which confirm that strong shape distortion of the polar vortex is not exhibited in any of the leading modes of variability.

We may summarize the transport model findings by using the European region during EVS cases, with strong local ozone reductions, as an illustration. Below about 200 hPa, the vertical advection contribution dominates the total ozone reduction. This can be understood as follows. In the strong upper tropospheric anticyclonic ridge, the potentially warm, ascending airmasses and associated high tropopause mean that a greater percentage than normal of the total ozone column is occupied by ozone poor tropospheric air. Furthermore, this leads to a general divergence of ozone rich stratospheric air out of local columns in the lower stratosphere. Hence, airmass ascent in connection with ageostrophic wind divergence plays a significant part in reducing ozone locally. In this respect, we note that Schmitz et al. (2000) have demonstrated the link between patterns of tropopause pressure change and those of ozone column trend for January.

Simultaneous to these vertical motions, the horizontal airflow in the upper troposphere has a south-westerly component to the west of Europe, advecting air from the sub-tropics towards the continent. Nevertheless, the transport model findings show that this has only a minimal and insignificant effect on the total ozone change here. However, the horizontal advection term is shown to play an increasing role at higher levels in the stratosphere. Here, the displaced polar vortex induces an anomalous north-westerly airflow into Europe. This also contributes to the local ozone decrease since the sign of meridional ozone gradients is opposite to those in the troposphere. Horizontal ozone gradients are clearly more significant in the stratosphere than lower down, simply because ozone concentrations are far greater there.

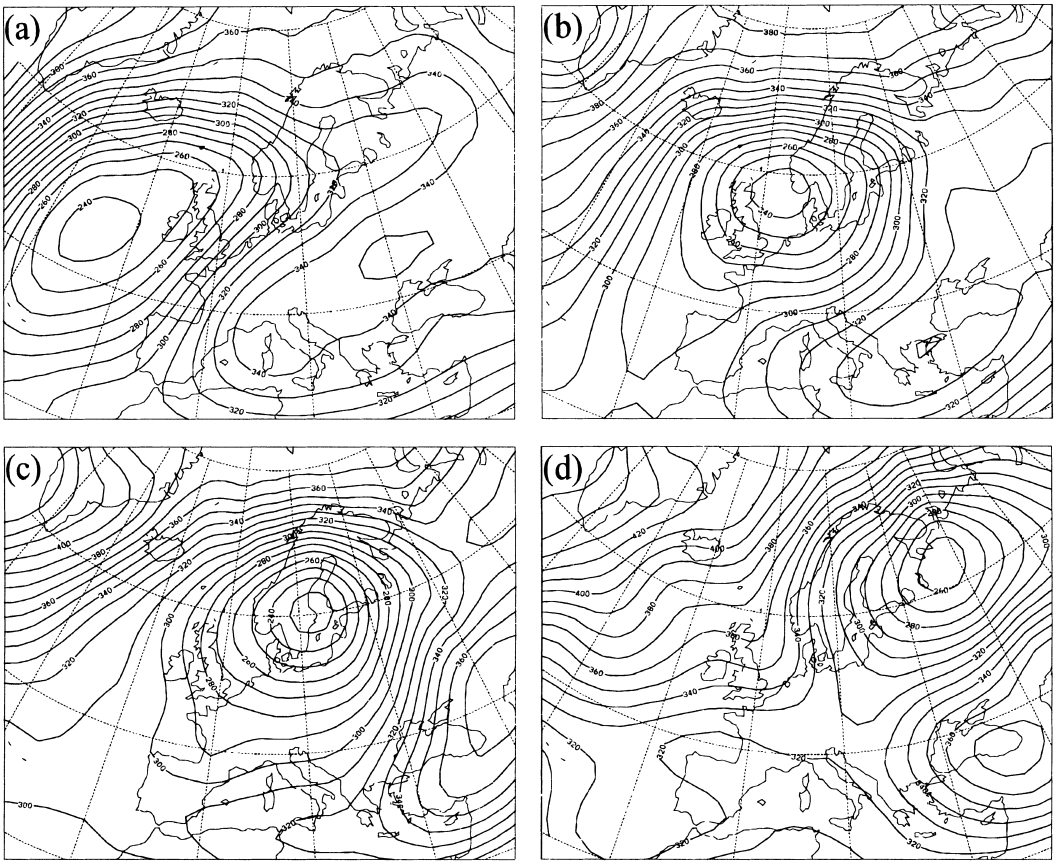

Fig. 7. Total ozone composite fields of subsets of the 10% of winter days between 1982 and 1992 when the phase of field-triplet-EOF 1 was most negative, taking only those days when an ozone mini-hole was also simultaneously in transit across the European region, grouping events into 4 sub-composites depending on the mini-hole location: namely, mini-holes near the longitudes, (a) 20°W (8 days), (b) 5°E (9 days), (c) 20°E (8 days), (d) 40°E (7 days). Contour interval 10 DU.

The greatest local changes in column total ozone levels occur, therefore, when the whole circulation pattern works together to yield a coherent, positively correlated relationship between the horizontal and vertical advection contributions to ozone changes. Presumably, neither upper tropospheric anticyclonic ridging without polar vortex displacement, nor a shifted polar vortex without a tropospheric ridge could produce such a strong ozone reduction. However, the field-triplet EOF analysis, picking out modes of variability linking the upper tropospheric geopotential, polar vortex and total ozone, has confirmed that dynamically coherent circulation patterns, optimal for leading to strong ozone reductions, especially over the European region, are indeed common for the northern hemisphere.

Considering further the special case of ozone mini-holes, we note that whenever a baroclinic wave passes through a region of already strongly depleted ozone, the potential for transient very low ozone values is enhanced. To illustrate this for the European region, we examine all days when the phase of the field-triplet-EOF 1 was most negative, relating to a strong general ozone reduction over Europe. We select the lowest 10% of amplitudes of this EOF 1 pattern, yielding 90 days from the ten years of winter data. Of these days, a further selection is made, only including those days when a strong ozone mini-hole was

located somewhere within the region, based on the mini-hole climatology dataset of James (1998). By grouping these events further by mini-hole location, a set of composite ozone fields are produced, showing the typical mean passage of ozone mini-holes through the region of strong ambient ozone reduction, Fig. 7. Each picture is a composite of typically about 8 events. The averaged mini-hole tracks in an east-north-eastward direction from west of the British Isles (a), across the central North Sea (b), to the southern half of Scandinavia (c), where its amplitude peaks at around 230 DU, before decaying over north-west Russia (d).

Our results are consistent with the observation of Petzoldt et al. (1994) and Petzoldt (1999) that the most intense European mini-holes tend to occur in combination with a strong, displaced European–Siberian polar vortex. However, with the help of our linear transport model, we are able to demonstrate, for the first time, the dynamical relationships behind this observation, showing how the nature of the 3D ozone structure and its interaction with ultra-long waves at various levels leads to strong local ozone reductions, which can then be enhanced temporarily to exceptional intensities during the transit of baroclinic waves.

7. Acknowledgements

We wish to thank the Deutscher Wetterdienst (DWD) and Deutsches Klimarechenzentrum (DKRZ) for providing us with the ECMWF-Reanalysis data. The invaluable work performed by the Ozone Processing Team at the NASA/Goddard Space Flight Center, Greenbelt, USA in making the TOMS gridded ozone data available to us is greatly appreciated. P. James would like to thank the German Federal Ministry for Education and Research (BMBF), within the context of its Ozone Research Programme (OFP), for their financial support of project number 01 LO 9510/5. We thank G. Schmitz for discussions which have helped to improve the manuscript.

REFERENCES

Dobson, G. M. B., Harrison, D. N. and Lawrence, J. 1929. Measurements of the amount of ozone in the earth's atmosphere and its relation to other geophysical conditions: Part III. *Proc. Roy. Soc. London* **A122**, 456–486.

Ertel, H. 1942. Ein neuer hydrodynamischer Wirbelsatz, *Meteor. Z.* **59**, 277–281.

Graf, H.-F., Kirchner, I. and Perlwitz, J. 1998. Changing lower stratospheric circulation: the role of ozone and greenhouse gases. *J. Geophys. Res.* **103**, D10, 11251–11261.

Greisiger, K. M., Peters, D., Entzian, G. and Hinrichs, C.-O. 1998. The mid-latitude horizontal and vertical structure of the zonally asymmetric intraseasonal and interannual ozone variability in boreal winters. *Climate Dynamics* **14**, 891–904.

James, P. M., Peters, D. and Greisiger, K. M. 1997. A study of ozone mini-hole formation using a tracer advection model driven by barotropic dynamics. *Meteorol. Atmos. Phys.* **64**, 107–121.

James, P. M. 1998. A climatology of ozone mini-holes over the northern hemisphere. *Int. J. Climatol.* **18**, 1287–1303.

Kurzeja, R. J. 1984. Spatial variability of total ozone at high latitudes in winter. *J. Atmos. Sci.* **41**, 695–697.

McIntyre, M. E. and Palmer, T. N. 1983. Breaking planetary waves in the stratosphere. *Nature* **305**, 593–600.

McKenna, D., Jones, R. L., Austin, J., Browell, E. V., McCormick, M. P., Krueger, A. J. and Tuck, A. F. 1989. Diagnostic studies of the Antarctic vortex during the 1987 Airbourne Antarctic Ozone Experiment: Ozone mini-holes. *J. Geophys. Res.* **94**, 11641–11668.

McPeters, R. D., Heath, D. F. and Bhartia, P. K. 1984. Average ozone profiles for 1979 from NIMBUS 7 SBUV instrument. *J. Geophys. Res.* **89**, 5199–5214.

Newman, P. A., Lait, L. R. and Schoeberl, M. R. 1988. The morphology and meteorology of southern hemisphere Spring total ozone mini-holes. *Geophys. Res. Let.* **15**, 923–926.

Peters, D. and Entzian, G. 1999. Longitude-dependent decadal changes of total ozone in boreal winter months during 1979–1992. *Journal of Climate* **12**, 1038–1048.

Peters, D., Egger, J. and Entzian, G. 1995. Dynamical aspects of ozone mini-hole formation. *Meteorol. Atmos. Phys.* **55**, 205–214.

Peters, D., Entzian, G. and Schmitz, G. 1996. Ozone anomalies over the North Atlantic–European region during January 1979–1992, linear modeling of horizontal and vertical ozone transport by ultra-long waves. *Beitr. Phys. Atmos.* **69**, 477–489.

Petzoldt, K. 1999. The role of dynamics in total ozone deviations from their long-term mean over the northern hemisphere. *Ann. Geophysicae* **17**, 231–241.

Petzoldt, K., Naujokat, B. and Neugebohren, K. 1994. Correlation between stratospheric temperature, total ozone and tropospheric weather systems. *Geophys. Res. Lett.* **21**, 1203–1206.

Plumb, R. A. et al. 1994. Intrusions into the lower stratospheric arctic vortex during the winter of 1991/92. *J. Geophys. Res.* **99**, 1089–1106.

Randel, J. W. 1992. Global atmospheric circulation statistics, 1000–1 mb. *NCAR, TN 366 + STR*. NCAR Technical Note, Boulder, CO.

Reed, R. J. 1950. The role of vertical motions in ozone — weather relationships. *J. Met.* **7**, 263–267.

Rood, R. B., Nielsen, J. E., Stolarski, R. S., Douglas, A. R., Kaye, J. A. and Allen, D. J. 1992. Episodic total ozone minima and associated effects on heterogeneous chemistry and lower stratospheric transport. *J. Geophys. Res.* **97**, 7979–7996.

Scherhag, R. 1952. Die explosionsartige Stratosphärenerwärmungen des Spätwinters 1951/52. *Berichte des Deutschen Wetterdienstes in der US-Zone* **6**, nr. 38, 51–63.

Shindell, D. T., Miller, R. L., Schmidt, G. A. and Pandolfo, L. 1999. Simulation of recent northern winter climate trends by greenhouse-gas forcing. *Nature* **399**, 452–455.

Schmitz, G., Peters, D. and Entzian, G. 2000. Tropopause pressure change in January during 1979–1992. *Meteorol. Z.* **9**, in press.

Thompson, D. W. J. and Wallace, J. M. 1998. The Arctic oscillation signature in the wintertime geopotential height and temperature fields. *Geophys. Res. Lett.* **25**, 1297–1300.

Waugh, D. W. 1997. Elliptical diagnostics of stratospheric polar vortices. *Q. J. R. Meteorol. Soc.* **123**, 1725–1748.

Waugh, D. W. and Randel, W. J. 1999. Climatology of Arctic and Antarctic polar vortices using elliptical diagnostics. *J. Atmos. Sci.* **56**, 1594–1613.